J. Fluid Mech. (1995), *vol.* 282, *pp.* 1–20
Copyright © 1995 Cambridge University Press

Surface quasi-geostrophic dynamics

By ISAAC M. HELD[1], RAYMOND T. PIERREHUMBERT[2], STEPHEN T. GARNER[1] AND KYLE L. SWANSON[2]

[1] Geophysical Fluid Dynamics Laboratory/NOAA, Princeton University, Princeton, NJ 08542, USA

[2] Department of Geophysical Sciences, University of Chicago, Chicago, IL 60637, USA

(Received 2 March 1994 and in revised form 14 July 1994)

The dynamics of quasi-geostrophic flow with uniform potential vorticity reduces to the evolution of buoyancy, or potential temperature, on horizontal boundaries. There is a formal resemblance to two-dimensional flow, with surface temperature playing the role of vorticity, but a different relationship between the flow and the advected scalar creates several distinctive features. A series of examples are described which highlight some of these features: the evolution of an elliptical vortex; the start-up vortex shed by flow over a mountain; the instability of temperature filaments; the 'edge wave' critical layer; and mixing in an overturning edge wave. Characteristics of the direct cascade of the tracer variance to small scales in homogeneous turbulence, as well as the inverse energy cascade, are also described. In addition to its geophysical relevance, the ubiquitous generation of secondary instabilities and the possibility of finite-time collapse make this system a potentially important, numerically tractable, testbed for turbulence theories.

1. Introduction

The two-dimensional flow of an incompressible fluid is governed by the vorticity equation

$$\partial_t \zeta = -J(\psi, \zeta), \tag{1a}$$

where

$$\zeta \equiv (\partial_{xx} + \partial_{yy})\psi, \tag{1b}$$

$$J(A, B) \equiv [(\partial_x A)\partial_y B - (\partial_x B)\partial_y A]. \tag{1c}$$

This equation and its variants have proved useful in meteorology, oceanography and magnetodynamics. But interest has also been generated for more abstract reasons: the 'turbulent' flows that it produces have a flavour that is quite distinct from those produced by the three-dimensional Euler equations; and it is much more computationally tractable than its three-dimensional counterpart.

This paper is devoted to a fluid dynamical system with a very similar formal structure, describing the evolution of a surface buoyancy or temperature field in a rapidly rotating, stratified, uniform potential vorticity fluid. The equations take the form

$$\partial_t \Theta = -J(\psi, \Theta), \quad z = 0, \tag{2a}$$

$$\Theta \equiv \partial_z \psi, \tag{2b}$$

$$(\partial_{xx} + \partial_{yy} + \partial_{zz})\psi = 0, \quad z > 0, \tag{2c}$$

$$\psi \to 0 \quad \text{as} \quad z \to \infty. \tag{2d}$$

A scalar is once again advected in two dimensions by a non-divergent flow whose structure is determined by that scalar, but with a different relation between the flow and the scalar field. Here this relationship is determined by solving Laplace's equation for

$z > 0$ with the Neumann boundary condition along $z = 0$ provided by the advected scalar. In the following, we refer to the solutions to (1) as two-dimensional Euler, or simply two-dimensional, flows, and the solutions to (2) as surface quasi-geostrophic, or SQG, flows.

Our motivation for studying (2) is partly geophysical, in that there are potential meteorological and oceanic applications. But it is again partly mathematical, in that SQG flows have characteristics that are sharply distinguished from the solution to (1) while retaining the computational advantages of a two-dimensional system. Some of these characteristics, such as nonlinear interactions that are more local in the spectral domain, and the potential for the formation of finite-time singularities, give SQG flows a flavour that is intermediate between the two- and three-dimensional Euler equations. Thus, study of this system can be justified on physical grounds as well as by the hope that it will provide a useful testing ground for turbulence theories more generally. Our approach in this paper is to touch upon a series of problems that illustrate some of the characteristics of SQG flows, without detailed analysis, so as to motivate more detailed studies.

2. Basic equations

Quasi-geostrophic (QG) theory describes the evolution of the departures from solid-body rotation in a rapidly rotating, stably stratified fluid. In its Boussinesq version, the flow evolves according to the coupled vorticity (ζ) and buoyancy (Θ) equations:

$$\partial_t \zeta = -J(\psi, \zeta) + f\partial_z w, \tag{3a}$$

$$\partial_t \Theta = -J(\psi, \Theta) - N^2 w, \tag{3b}$$

$$\Theta \equiv f\partial_z \psi. \tag{3c}$$

Here ψ is the streamfunction for the horizontal geostrophic flow, $(u, v) = (-\psi_y, \psi_x)$, w is the vertical motion, f is the constant vorticity due to the background rotation, while $N(z)$ is the buoyancy frequency of a reference state. The vorticity is defined as in two-dimensional flow (1b). Eliminating the vertical motion, one obtains the pseudo-potential vorticity equation

$$\partial_t q = -J(\psi, q); \quad q \equiv (\partial_{xx} + \partial_{yy} + \partial_z \epsilon \partial_z)\psi; \quad \epsilon \equiv (f/N)^2. \tag{4}$$

If we specialize to the case of constant N, the factor ϵ can be subsumed into a rescaled vertical coordinate, Nz/f (in which case we retain the notation z for the rescaled coordinate), and the potential vorticity is now simply the three-dimensional Laplacian of the streamfunction.

At a flat lower boundary, the condition of no normal flow is

$$\partial_t \Theta = -J(\psi, \Theta), \quad z = 0. \tag{5}$$

In the presence of a surface with elevation $h(x, y)$, vertical advection across the mean density gradient leads to the modification

$$\partial_t \Theta = -J(\psi, \Theta + N^2 h), \tag{6}$$

but consistent with quasi-geostrophic scaling this boundary condition is still applied at $z = 0$. If a flat upper boundary is imposed, then (5) also holds at $z = H$.

The familiar special case of two-dimensional flow is obtaining by assuming that the streamfunction is independent of z and, if $h \neq 0$, setting $N^2 \equiv 0$. A less familiar special case is that of SQG flow, in which it is assumed that $q \equiv 0$, so that the interior equation is identically satisfied, and the flow is driven entirely by the surface Θ-distribution. If the surface is flat, if N^2 is a constant, and if there is no upper boundary, then the

resulting equations are as displayed in the introduction, where we have subsumed the constant f into the definition of Θ. Solutions are assumed to decay as $z \to \infty$. In the presence of orography, (2*a*) is replaced by (6). If $q = 0$, but with non-constant N^2, the dynamics is unaltered qualitatively, but the elliptic equation to be solved, replacing (2*c*), has non-constant coefficients.

One can easily generalize to the case of $q = q_0$, a non-zero constant. For example, in the presence of a uniform horizontal shear, with the total flow described by the streamfunction $\frac{1}{2}q_0 y^2 + \psi$, one need only incorporate advection by the mean flow, $u = -q_0 y$, into the buoyancy equation.

Generalization to the non-Boussinesq case is also straightforward. For an ideal gas over a flat surface, Θ is now interpreted as the surface potential temperature, which is again conserved following the non-divergent geostrophic flow, but with

$$\Theta \equiv \partial_z \psi - (\kappa/H)\psi, \quad z = 0, \tag{7a}$$

$$0 = (\partial_{xx} + \partial_{yy})\psi + \rho^{-1} f^2 \partial_z (\rho N^{-2} \partial_z \psi), \quad z > 0, \tag{7b}$$

$$\rho \equiv \exp(-z/H). \tag{7c}$$

Here $\kappa \equiv (c_p - c_v)/c_p$ ($\approx 2/7$ for air), where c_p and c_v are the heat capacities at constant pressure and volume, and H is the scale height of a reference atmosphere.

One can always divide the total flow at any instant into a part induced by the surface Θ-distribution and a part induced by the interior q-distribution. There are meteorological problems for which the former is thought to predominate, motivating the analysis of this special case. Schar & Davies (1990) use this model to discuss aspects of cyclone development, while Smith (1984) uses it to analyse the generation of cyclones by isolated orography. (Schar & Davies actually consider the geostrophic momentum rather than quasi-geostrophic equations – see §5.) Blumen (1978) has presented the Kolmogorov–Kraichnan scaling arguments for the spectral shapes expected in this model's turbulent inertial ranges, and these have recently been compared with numerical simulations by Pierrehumbert, Held & Swanson (1994, referred to as PHS in the following). Hoyer & Sadourny (1982) discuss turbulent closure theory for the more general Eady problem (with two surfaces), and multifractal characterization of the inertial range SQG vorticity has been pursued in Pierrehumbert (1994). Constantin, Majda & Tabak (1994) study singularity formation in this model.

Introducing an environmental horizontal buoyancy gradient in the flat-bottomed case, analogous to the β-effect in two-dimensional flow, results in

$$\partial_t \Theta = -J(\psi, \Theta + \Lambda y). \tag{8}$$

The constant Λ can equivalently be thought of as due to a background vertical shear in the x-component of the flow, $f\partial_z u = -\Lambda$. As this contributes nothing to the interior potential vorticity, the interior equation is unaltered. This system now supports linear waves with the dispersion relation

$$\omega = -\Lambda k/K, \tag{9}$$

where $\psi = \mathrm{Re}\, \Psi e^{i(kx+ly-\omega t)}$, $K^2 = k^2 + l^2$. (This should be contrasted with the familiar Rossby wave dispersion relation, $\omega = -\beta k/K^2$.) These are edge waves that decay away from the surface as e^{-Kz}. The interaction between two such waves, one at the surface and another at the tropopause, gives rise to baroclinic instability in Eady's (1949) classic model of that process. Eady edge waves are identical dynamically to topographic edge waves, of importance in oceanography, where the buoyancy gradient at the surface is caused by a sloping lower boundary (as in (6)) rather than a horizontal temperature gradient. More abstractly, (8) provides a model for the interaction

between waves and turbulence that can serve as a counterpoint to that provided by two-dimensional flow.

The model (2) can also be obtained from the full quasi-geostrophic model in a region removed from any boundaries, in the case that N is a discontinuous function of z, an approximation that is often made when modelling the tropopause. Assuming that $q = 0$ everywhere except at the location of this discontinuity (at $z = z_c$), so that the flow decays away from z_c on both sides, one finds by integrating across the discontinuity that

$$\partial_t \Delta = -J(\psi, \Delta), \tag{10a}$$

where

$$\Delta \equiv (\partial_z \psi / N^2)^+ - (\partial_z \psi / N^2)^-. \tag{10b}$$

Since

$$\Delta(z_c) = \{(N^+ + N^-) K/f\} \Psi(z_c) \tag{11}$$

for a wave with horizontal wavenumber K, this problem reduces to SQG after rescaling coordinates. Aspects of linear edge wave dynamics at the tropopause have been examined by Rivest, Davies & Farrell (1992) and Rivest & Farrell (1992). Juckes (1994) has recently argued the case for the relevance of SQG for tropopause dynamics. Some limitations of this model of the tropopause are illustrated in Garner, Nakamura & Held (1992).

Finally, we note that even if N^2 is independent of height, one can still generate a horizontal surface in the interior on which SQG dynamics is obeyed, by assuming that the vertical shear $\partial_z u$ is initially a discontinuous function of height.

3. Two-dimensional versus SQG

Some of the distinctions between SQG and two-dimensional flows are immediately evident from the form of the equations.

In two-dimensional flow, the streamfunction induced by a point vortex, $\zeta = \delta(\boldsymbol{x}')$, in an unbounded domain is $\psi(\boldsymbol{x}) = -(2\pi)^{-1} \ln(|\boldsymbol{x} - \boldsymbol{x}'|)$. In SQG flow, $\Theta = \delta(\boldsymbol{x}')$ results in the flow $\psi(\boldsymbol{x}) = -(2\pi |\boldsymbol{x} - \boldsymbol{x}'|)^{-1}$. The circumferential velocities around the vortex are proportional to r^{-1} for two-dimensional flow and r^{-2} for SQG flow, r being the distance from the vortex centre.

The more singular SQG Green's function has several important consequences. Nearby point vortices rotate about each other more rapidly than in the two-dimensional case; in consequence, a greater ambient strain is required to pull them apart, since the rapid rotation averages out the effects of the strain. Conversely, distant eddies are less tightly bound to each other than in two-dimensional flow. Taken together, a greater tendency to form localized vortex assemblages is implied. Since the flow dies away from a point vortex as r^{-2} rather than r^{-1} in SQG, the aggregate effect of distant eddies on the local velocity field is more limited. SQG is qualitatively characterized by the preponderance of spatially local rather than long-range interactions.

In terms of spectral amplitudes, if $\psi = \mathrm{Re}(\Psi_{\boldsymbol{K}} e^{i\boldsymbol{K}\cdot\boldsymbol{x}})$ in two-dimensional flow, then $\zeta = \mathrm{Re}(Z_{\boldsymbol{K}} e^{i\boldsymbol{K}\cdot\boldsymbol{x}})$ with

$$Z_{\boldsymbol{K}} = -|\boldsymbol{K}|^2 \Psi_{\boldsymbol{K}}. \tag{12}$$

Since the vertical structure of a sinusoidal disturbance in SQG theory is $e^{-|\boldsymbol{K}|z}$, the analogous relation is

$$\Theta_{\boldsymbol{K}} = -|\boldsymbol{K}| \Psi_{\boldsymbol{K}}. \tag{13}$$

In both models, the flow can be thought of as determined by a smoothing operator acting on the conserved scalar, but in SQG there is less smoothing. This implies that large-scale strain will play a relatively smaller role in the advection of small-scale

features in SQG, resulting in a cascade of variance to small scales that is more local in wavenumber. This matter is discussed in Hoyer & Sadourny (1982) and PHS. The sort-range SQG interactions also suggest that strong deviations from the predictions of mean field theory (see Miller 1990 for the two-dimensional case) are to be expected.

A step discontinuity of vorticity implies a discontinuity in velocity gradient, but velocities remain finite and continuous. In consequence, for two-dimensional flow uniform-vorticity patches are quite well-behaved, and 'contour dynamics', in which the vorticity distribution is approximated by such patches, has proven to be a useful computational approach (Dritschel 1989*a*, and references therein). Homogenization of potential vorticity figures prominently in many physical problems, with the sharp vorticity interfaces produced at the edge of mixed regions being rather inactive (see Rhines & Young 1982 and Pierrehumbert 1991 for oceanic and atmospheric examples, respectively). Homogenization in the SQG system is expected to proceed differently, given that the tangential velocity diverges logarithmically in the vicinity of a step discontinuity in Θ.

To better appreciate the nature of the singularity, consider a curve Γ with $\Theta = 1$ inside and $\Theta = 0$ outside. By integrating the Green's function over the path, the velocity at $(x = 0, y = 0)$ on the boundary is

$$u\boldsymbol{e}_x + v\boldsymbol{e}_y = (2\pi)^{-1} \int_\Gamma (\boldsymbol{e}_x \, \mathrm{d}x' + \boldsymbol{e}_y \, \mathrm{d}y')/(x'^2 + y'^2)^{1/2}, \tag{14}$$

where $\boldsymbol{e}_x$ and $\boldsymbol{e}_y$ are unit vectors in the x- and y-directions. If the boundary is twice differentiable, we can adopt local coordinates such that $y' = \frac{1}{2}bx'^2$. Substituting into (14), the contribution from the local, singular portion of the integral is, to leading order,

$$u\boldsymbol{e}_x + v\boldsymbol{e}_y = (2\pi)^{-1} \int_{\Gamma'} \mathrm{d}x' (\boldsymbol{e}_x/|x'| + \boldsymbol{e}_y bx'/|x'|), \tag{15}$$

where Γ' represents the portion of the curve near $(0, 0)$. According to (15), the *tangential* velocity u is divergent, but the local contribution to the *normal* velocity v (which is what displaces the bounding curve) actually vanishes to leading order. As a result, the evolution of such a discontinuity can be relatively benign, despite the infinite tangential velocities. (Waugh & Dritschel 1991 have studied contour dynamics for a range of Green's functions, but not with singularities as strong as SQG.)

For smooth initial conditions, the two-dimensional Euler equations cannot form singular vorticity gradients in finite time (Rose & Sulem 1978, and references therein). This has also been demonstrated for QG dynamics in the special case when Θ is constant on the boundaries (Bennett & Kloeden 1980, 1982). Bennett & Kloeden point out, however, that their proof breaks down when there are non-zero boundary temperature gradients, admitting the possibility of finite-time singularity formation. SQG is the natural simplest case in which to study the possibilities for breakdown. Hoyer & Sadourny estimate the breakdown time as $fL/\delta\Theta$, where L is the characteristic lengthscale and $\delta\Theta$ the characteristic buoyancy perturbation. Recently, Constantin *et al.* (1994) have presented detailed numerical evidence for finite-time collapse in SQG. They argue that the simple initial condition

$$\Theta = \cos(y) + \sin(x)\sin(y) \tag{16}$$

forms a cusp in the temperature field at $t = t_c \approx 8.5$, with the magnitude of the temperature gradient $\propto (t - t_c)^{-7/4}$. The SQG system, once desingularized by the addition of a suitably scale-selective dissipation, should provide a useful model for examining the interaction of nearly singular structures with large-scale flows.

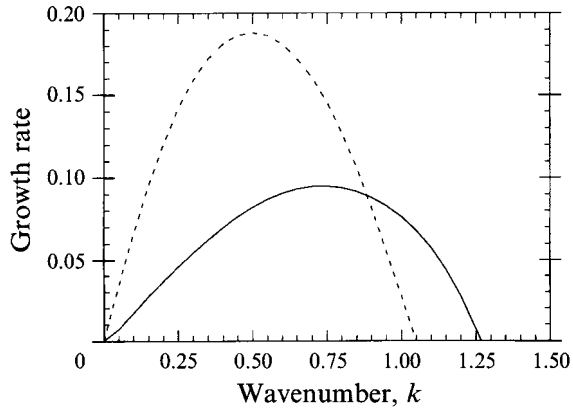

FIGURE 1. Growth rates for a Gaussian temperature filament in SQG (——) compared with those for a vorticity filament in two-dimensional flow (– – –). In both cases, the wavenumber is non-dimensionalized by L^{-1}. Growth rates are non-dimensionalized by BL^{-1} for SQG and by Z for two-dimensional flows (see (18)).

It should be emphasized that the formation of a step discontinuity in Θ is not energetically precluded in SQG. The conserved energy in this system is the kinetic plus available potential energy in the three-dimensional domain, $z > 0$:

$$\int\int\int_{z>0} \mathrm{d}x\,\mathrm{d}y\,\mathrm{d}z\,(u^2+v^2+\Theta^2/N^2)/2. \tag{17}$$

The logarithmic singularity in the tangential velocities is integrable. Furthermore, if the discontinuity lies along a line, then it is stable, as is any monotonic distribution $\Theta(y)$. The stability can be inferred as a special case of the Charney–Stern–Pedlosky criterion (Pedlosky 1979), which for SQG states that instability is precluded unless $\partial_y \Theta$ changes sign. Hence the singular character of SQG interfaces cannot lead to the large-scale rollup typical of vortex sheets in two-dimensional flow.

The simplest unstable configuration is that of a temperature *filament*, analogous to a vorticity filament in two-dimensional flow. In the two-dimensional case, the parallel flow defined by

$$\zeta = Z\exp(-(y/L)^2), \tag{18a}$$

for example, is unstable, with the most unstable wavelength proportional to L, and the growth rate proportional to the magnitude of the vorticity, Z. The analogous parallel SQG flow, with

$$\Theta = B\exp(-(y/L)^2), \tag{18b}$$

is also unstable. (A closely related problem is treated by Schar & Davies 1990.) The most unstable wavelength again scales with L, but the growth rates are proportional to BL^{-1}. This is the magnitude of the vorticity in the associated shear flow, which is the only available timescale. The non-dimensional growth rate spectra for the Gaussian filament in two-dimensional and SQG flows are compared in figure 1.

The scaling of the growth rates of filamentary instabilities has important implications. The shedding and stretching of vorticity filaments is a generic feature of two-dimensional flows (e.g. Dritschel 1988; Pierrehumbert 1991, and references therein). As a filament is stretched, the growth rate of secondary instabilities on this filament remains constant, since vorticity is conserved. As a result, the filament is relatively easily stabilized by larger-scale shears and strains induced by remote vorticity distributions, as these need only be of the same order of magnitude as the shear induced

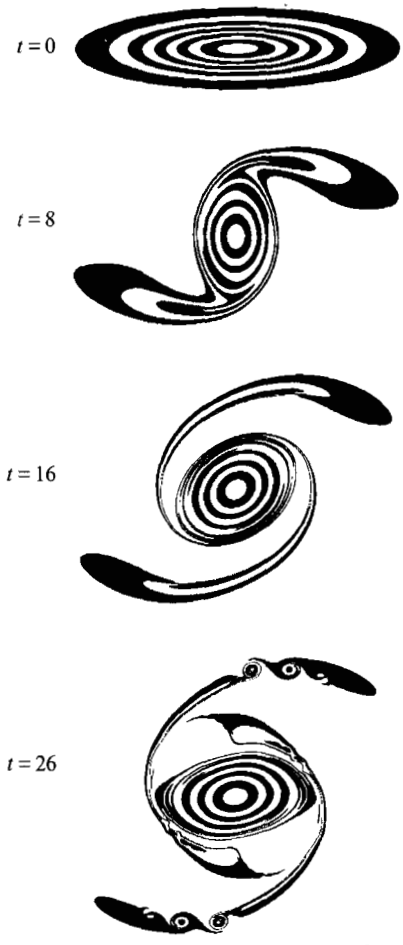

FIGURE 2. Evolution of ellipse with eccentricity of 4 in SQG. Temperature is shown at times $t = 0, 8, 16, 26$.

by the filament itself (see Dritschel 1989*b*; Waugh & Dritschel 1991). In the SQG case, in contrast, it is the temperature within the filament that is conserved, while the vorticity, and the growth rate of the instability, increase as the filament is stretched and thinned. Whatever environmental strains that exist will eventually be overcome, and the instability of the filament is inevitable. The inevitability of this secondary instability provides an alternative way of seeing that the cascade of variance to small scales in SQG is spectrally local (PHS). These instabilities should in turn lead to further filamentation and instability, resulting in the 'curdling' of the filament on ever finer scales.

4. Examples

4.1. *An elliptical vortex*

In our first illustrative example of SQG flow, the initial condition is the smooth elliptical distribution

$$\Theta|_{t=0} = \exp(-x^2-(4y)^2). \tag{19}$$

As shown in figure 2, filaments are shed by the spinning vortex. By $t = 26$, instabilities are clearly seen on the outer filament, with other small-scale structure closer to the

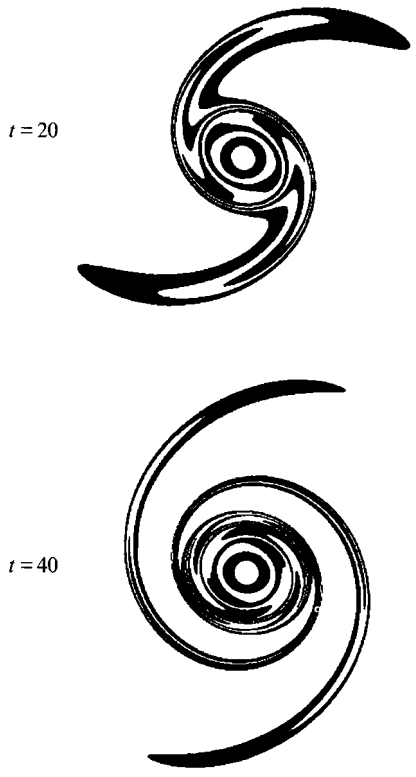

FIGURE 3. Vorticity in two-dimensional flow in which the initial condition in vorticity is identical to the initial condition for temperature in the SQG flow of figure 1, at $t = 20$ and 40.

vortex barely resolved. In the two-dimensional flow of figure 3, the same initial condition is chosen for ζ. Filaments are again shed from the vortex as it settles into a more circular shape, but there is no sign of a shear instability along these filaments; evidently they have not been thrown far enough from the stabilizing adverse shear of the central vortex. Note also that the two-dimensional vortex has become quite symmetrical through the filamentation process, while the SQG vortex has retained more of its eccentricity.

This result and those to follow are obtained with a 512×512 doubly periodic spectral model. In the present case, the domain is square, with sides of length 2π, and small-scale mixing has been included as $\nu\nabla^8(T \text{ or } \zeta)$, with $\nu = 10^{-19}$. The details of the solution would be slightly different in an infinite domain and with a different type of dissipation. The filamentary instability is still not very well resolved: its wavelength increases as ν is increased.

4.2. *Flow over an isolated mountain*

As a second example, consider the start-up vortex generated by blowing a uniform wind over an isolated mountain. The SQG equation is (6). The mountain is specified by setting

$$N^2 h = \exp(-(x^2 - y^2)/r^2). \tag{20}$$

The initial condition is $\boldsymbol{v} = U\boldsymbol{e}_x$, with $U = 0.10$ and $r = 0.5$. (Dimensionally, $U/(NH) = 0.10$, where H is the height of the mountain.) The domain is once again doubly periodic with sides of length 2π. The air initially on the mountain warms

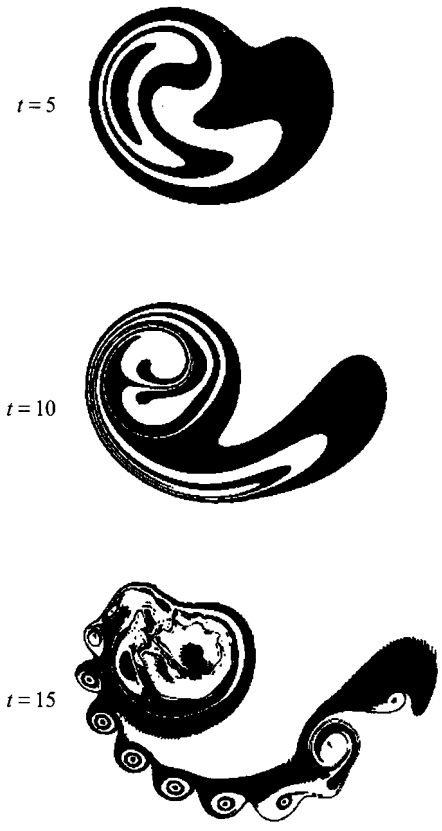

FIGURE 4. SQG flow over a Gaussian mountain, with $U/(NH) = 0.1$; surface potential temperature (the conserved quantity in (6)) is shown at $t = 5$, 10 and 15.

adiabatically as it descends, developing cyclonic vorticity, while the air replacing it cools, generating anticyclonic vorticity. As the flow evolves (figure 4), not only does the filament connecting the two vortices develop a well-defined instability, but a rich assortment of small-scale structures develops over the mountain. (This calculation was performed with $\nu = 10^{-19}$, and the solution does have a small amount of grid-scale noise. With a value of 10^{-18}, the number of vortices into which the main filament breaks is smaller.)

In the analogous two-dimensional flow (not shown), the initial evolution is similar, but the filament does not break up into vortices in the cases, and at the resolutions, that we have examined. Thompson & Flierl (1993) provide contour dynamics solutions to the two-dimensional problem for the case of a cylindrical mountain, confirming this picture.

4.3. *Filament instability*

As a third example, consider the finite-amplitude evolution of the instability of the filament (18), for which the linear growth rates have been shown in figure 1. The initial condition is

$$\Theta = \exp(-y^2)(1 + 0.05y\cos(kx)) \tag{21}$$

with $k = 0.8$, which is close to the most unstable wave.

A secondary instability is seen to develop after $t = 100$ (figure 5). The e-folding time and scale of this secondary rollup are consistent with the instability of a filament that has been stretched and thinned by a factor χ of about 100. We presume that a higher-

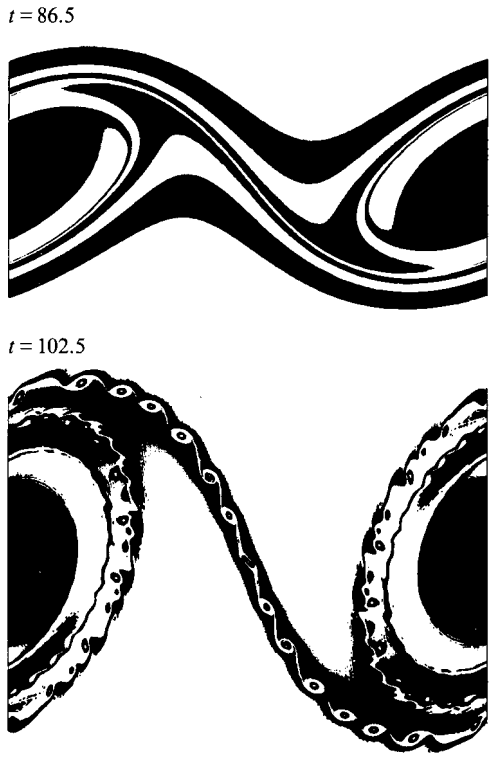

FIGURE 5. An unstable temperature filament, with the initial condition (21); temperatures shown at $t = 86.5$ and 102.5.

resolution computation would show a tertiary instability generated in an analogous way by the rollup of these secondary waves, but on time and space scales compressed by another factor of χ. One can imagine an infinite series of these instabilities developing in a self-similar fashion, with arbitrarily small spatial scales developing in the finite time obtained by summing the geometric series $\chi^{-1}+\chi^{-2}+\ldots$. In the analogous two-dimensional problem (not shown) the vortices that form from the initial instability twist the remnant vorticity filament around themselves, but no secondary instabilities are seen. The solution is very similar to that for a discontinuous strip of vorticity, for which we have contour dynamics solutions (e.g. Pozrikidis & Higdon 1985).

We suspect that this 'curdling' cascade of filamentary instabilities is a generic feature of SQG flows. The possibility of generating infinite local strains, as in the example of Constantin *et al.* (1994), as well as infinite secondary instability growth rates, creates a variety of possibilities. In particular, these secondary instabilities could be suppressed in regions where the amplifying strain is co-located with the thinning filament. We expect filament curdling to appear more clearly when the filament thinning is due to strain associated with remote temperatures.

4.4. *Edge wave critical layer*

Critical layers, locations where a wave's phase speed with respect to the ambient flow vanishes, play important roles in many geophysical flows, as they are locations of wave breaking and mixing. While Rossby wave critical layers have been studied intensively, we are unaware of any previous studies of the SQG edge wave critical layer.

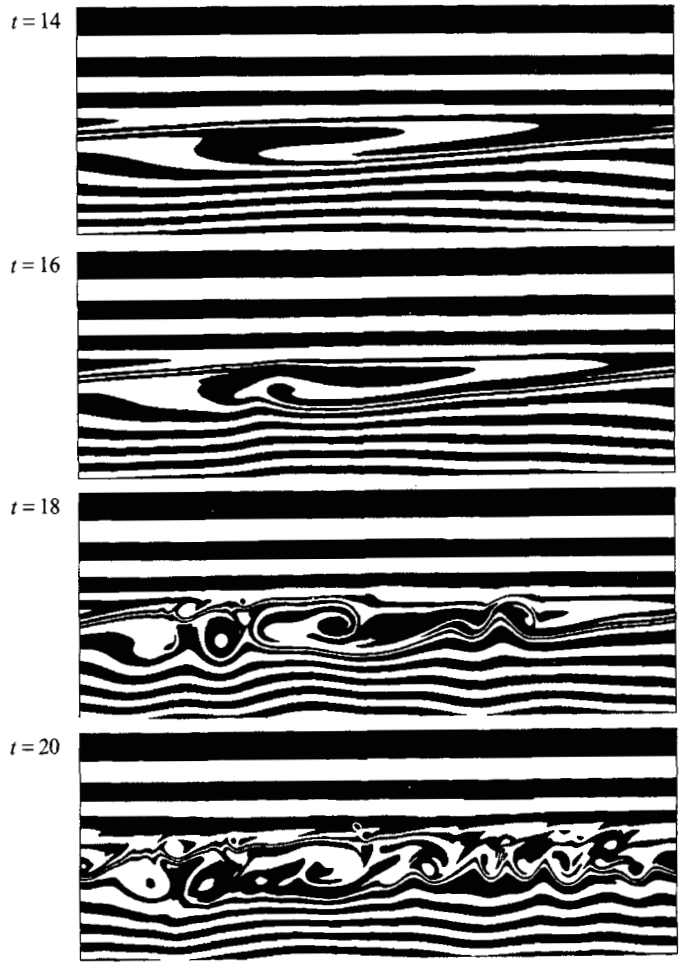

FIGURE 6. Evolution of temperatures in the edge wave critical layer (see text), at $t = 14$, 16, 18 and 20.

Start with a wave propagating on an environmental temperature gradient Λ, and assume also a constant meridional shear so that the basic state zonal wind is $U = -\Lambda z + \gamma y$. A linear disturbance to this flow satisfies

$$\partial_t \psi'_z = -\gamma y \psi'_{xz} + \Lambda \psi'_x, \quad z = 0, \tag{22a}$$

$$(\partial_{xx} + \partial_{yy} + \partial_{zz})\,\psi' = 0, \quad z > 0. \tag{22b}$$

For a stationary wave, $\partial_t = 0$, with $\psi' = \mathrm{Re}\{\Psi e^{ikx}\}$,

$$\gamma y \Psi_z = \Lambda \Psi, \quad z = 0. \tag{23a}$$

$$(-k^2 + \partial_{yy} + \partial_{zz})\,\Psi = 0, \quad z > 0. \tag{23b}$$

As the wave approaches its critical latitude at $y = 0$, the term involving the zonal wavenumber become negligible in (23), so that to leading-order Ψ satisfies Laplace's equation in the (y, z)-plane. An harmonic function that captures the leading singularity at $(0, 0)$ is

$$\Psi \propto \tan^{-1}(z/y) + \text{const.} \tag{24}$$

The streamfunction develops a jump discontinuity at $y = 0$, while the zonal velocity and the temperature are δ-functions to leading order. This is a more singular behaviour than occurs at a Rossby wave critical layer, for which $\Psi \approx y \ln(y) + \text{const.}$

For a first inspection of the nonlinear SQG critical layer using the doubly periodic spectral model, we choose a rectangular domain (L_x, L_y) and the initial condition $\Theta = \alpha \sin(2\pi y/L_y)$, which produces eastward and westward zonal flows centred at $y = 0$ and $\frac{1}{2}L_y$ respectively, where $\alpha > 0$. We then incorporate a mean temperature gradient, $\Lambda < 0$. Since Λ is negative, edge waves propagate eastward with respect to the mean flow, so they can be stationary on the westward flow near $\frac{1}{2}L_y$. To force the stationary edge wave, we also include the topography

$$h = A \cos(2\pi x/L_x) \exp(-\mu(y - L_y/2)^2)\, g(t). \tag{25}$$

The function $g(t)$ increases linearly from 0 at $t = 0$ to 1 at $t = T_1$, after which it is held constant; instantaneous imposition of the topography would generate transients that obscure the stationary wave. A linear stationary wave is generated in the vicinity of this source, which then propagates to the critical latitudes at $y = \frac{1}{4}L_y$ and $\frac{3}{4}L_y$.

The evolution of the temperature field near $\frac{3}{4}L_y$ is shown in figure 6. The parameters are $A = 0.2$, $\Lambda = -10$, $\mu = (0.02)^{-2}$, $L_x = 2$, $L_y = 1$, $T_1 = 10$, and $\nu = 10^{-20}$, with ∇^8 diffusivity. The wave has just begun to overturn when it quickly breaks down, and the layer is then filled with small-scale structures in short order. Examination of the flow in the linear part of the domain shows that substantial reflection is occurring. Indeed, if the flow reaches a statistically steady state in which the width of the region of mixing does not expand in time, one can show, using methods similar to those in Killworth & McIntyre (1985), that the incident wave action is perfectly reflected. We see substantial generation of higher harmonics, more so than we expect from the Rossby wave analogue. (For an example of an analogous calculation in two dimensions, see Beland 1976.) We postpone an attempt at detailed comparison of nonlinear critical-layer wave breaking in the two-dimensional and SQG models, which would likely require more resolution within the critical layer itself.

4.5. *Mixing by a perturbed edge wave*

The critical-layer problem is a fairly complex setting in which to study edge wave breaking and mixing of surface temperature. A simpler flow is provided by a free, finite-amplitude wave perturbed by a smaller-scale disturbance. This example illustrates the nature of the coexistence of waves and turbulence in SQG, and also allows one to study how the progress of homogenization is affected by the somewhat singular dynamics of a step-discontinuity interface in SQG. This class of mixing problems is discussed at length in the two-dimensional Rossby wave case by Pierrehumbert (1991), to which the reader is referred for further background.

We consider an x-periodic channel of length 2π with walls at $y = 0$ and π, and employ the initial condition

$$\psi = A \cos(x) \sin(y) + \epsilon \cos(2x) \sin(2y), \tag{26a}$$

$$\Theta = \Lambda y - \sqrt{2} \cos(x) \sin(y) - \epsilon \sqrt{8} \cos(2x) \sin(2y). \tag{26b}$$

When $\epsilon = 0$, this leads to a travelling edge wave moving with phase speed $c = -\Lambda/\sqrt{2}$ as discussed in the introduction. It is readily shown from the Jacobian form of the nonlinearity that the undisturbed wave is an exact solution of the full nonlinear equations, in the absence of damping. When A is sufficiently large ($A > \Lambda/\sqrt{2}$), the streamlines for this travelling wave, in the reference frame comoving with c, produce

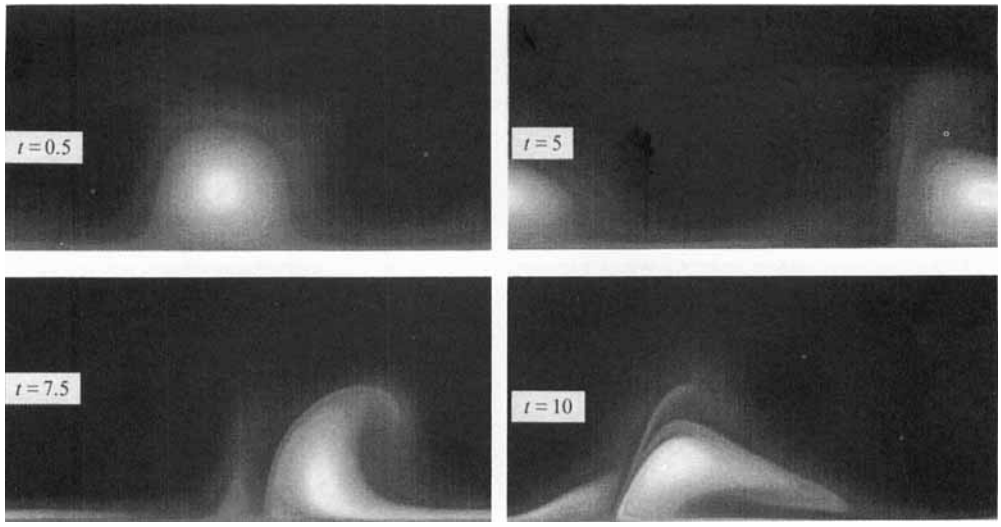

FIGURE 7. Initial evolution of temperatures in the perturbed edge wave, for $t = 0.5$, 5.0, 7.5 and 10.0.

a closed-streamline region bounded by a separatrix rooted in a pair of stagnation points; such structures, under perturbation, generically lead to chaotic mixing and ultimate homogenization of tracers within well-defined mixing regions extending outward from the separatrix as the strength of the perturbation is increased. The kinematic case (specified ψ) is discussed by Knobloch & Weiss (1987), Weiss & Knobloch (1988), and Pierrehumbert (1991). The dynamical case for two-dimensional flow is discussed by Pierrehumbert (1991). Here, we see how the dynamical case differs for SQG. In the dynamical case, the fluctuations necessary for mixing are not imposed externally, but instead arise naturally from the fact that the flow deviates from a steady solution (viewed in the comoving frame), when ϵ is non-zero.

We present simulations with $A = 1$, $\Lambda = 1$, and $\epsilon = 0.2$, carried out with 512×256 resolution, using ∇^{16} dissipation with coefficient 1.0×10^{-29}. Figure 7 shows the initial stages of the development of the Θ-pattern. Rapid gradient intensification is seen along the bounding streamline emanating from the leftmost stagnation point on the boundary. Exponential amplification of gradients is always expected in such problems, but there is indication of actual finite-time collapse to infinite gradients in this case, as in the simulation of Constantin *et al.* (1994). With dissipation as described, the integration proceeds through this time without any curdling. Filamentation and curdling are seen at later stages of the development.

The longer-term evolution is shown in figure 8. The development is characterized by the repeated formation of filaments as fluid is swept through the stagnation point. In the two-dimensional Euler case discussed in Pierrehumbert (1991), the filaments elongate and fold, leading ultimately to homogenization within certain mixing regions, but the folding is governed by the large-scale streamline pattern; there is little tendency for secondary rollup or small-scale curdling. A frame from the two-dimensional Euler calculation (case [1×2s] of Pierrehumbert 1991) is shown in figure 8. In contrast, as we have now come to expect, the filaments in the SQG case undergo a variety of secondary curdling and rollups at the tips.

The secondary instability has a spatially developing character, as can be seen especially well in figure 9. Filaments are created at the stagnation point, and the initial

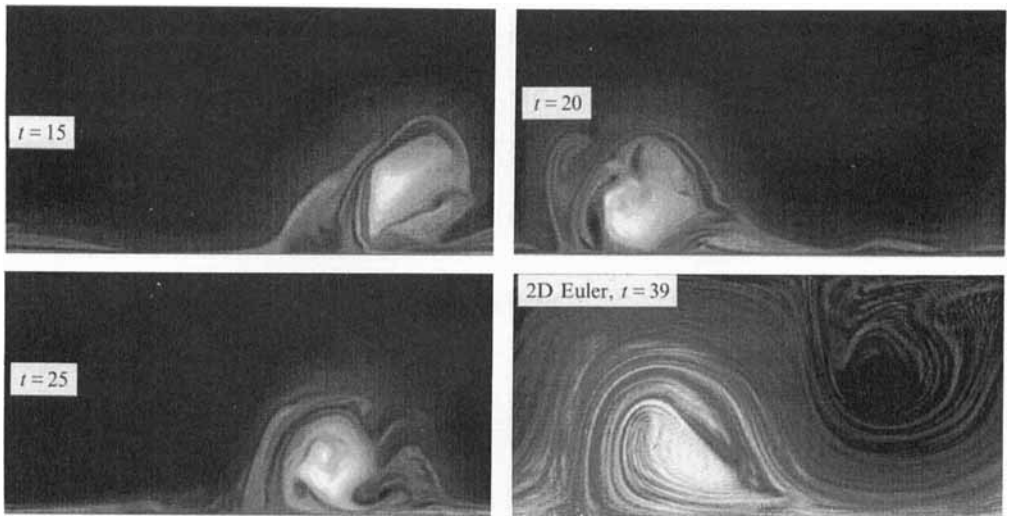

FIGURE 8. Further evolution of the perturbed edge wave, at $t = 15$, 20 and 25. Also shown is a snapshot of vorticity from the analogous calculation in two-dimensional flow, at $t = 39$.

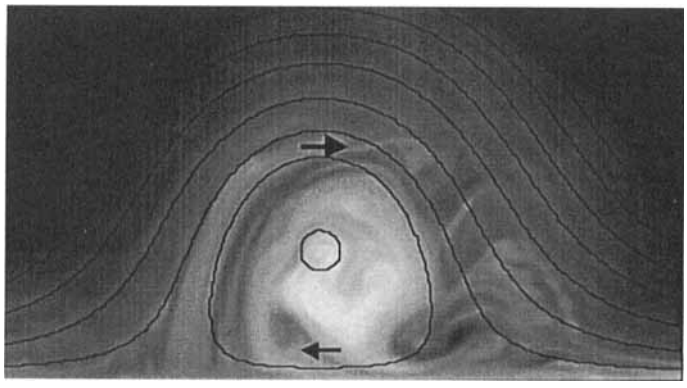

FIGURE 9. Close up of the perturbed edge wave at $t = 25$, with streamlines of the unperturbed wave.

stretch downstream of this point is smooth. Secondary instabilities amplify as they propagate along the filament. In consequence, there is a very 'turbulent' mixing region on the right-hand side of the eddy which is quite unlike the filamentary structure that predominates on the left. The cascade of temperature variance to small scales evidently has a dual character: sufficiently energetic large eddies can still exert a controlling influence over a range of scales (two orders of magnitude in this case), generating two-dimensional like filamentation, but with secondary instabilities eventually generating a local cascade.

Despite the fact that the filaments are less passive in SQG than in the two-dimensional case, the disposition of the mixing regions is still controlled by the large-scale streamline geometry. One still finds active mixing regions centred on the lower and upper eddies, separated by a sinuous mixing barrier that snakes through the central portions of the domain. Curdling in SQG makes the mixing more diffusive in character, by decreasing the correlation length of the velocity (analogous to the mean free path in kinetic theory). In doing so, it makes the mixing less effective than the

stretch and fold mixing that predominates in chaotic advection and two-dimensional Euler flows. Although we have not quantified the distinction, our impression is that homogenization is more difficult to obtain in SQG than in two-dimensional flows.

As in two-dimensional Euler flows, the mixing does not destroy the wave. Rather, the large-scale wave sweeps up the energy of the perturbation, and thereafter continues to propagate in an orderly fashion, a particular instance of the inverse energy cascade.

5. Turbulence

As described by Blumen (1978), Juckes (1994) and PHS, SQG dynamics possesses two quadratic conservation laws, analogous to energy and enstrophy consideration in two-dimensional flows:

$$V = \{\Theta^2\} \quad \text{and} \quad E = -\{\psi\Theta\}. \tag{27}$$

Curly brackets denote an average over the domain. E is the kinetic plus potential energy of the flow in three dimensions (see (17) above). Setting

$$V = \int v(k)\,\mathrm{d}k \quad \text{and} \quad E = \int e(k)\,\mathrm{d}k, \tag{28}$$

the Kolmogorov–Kraichnan theory predicts two inertial ranges for homogeneous isotropic turbulence, one at high wavenumbers through which V cascades to smaller scales, with $v(k) \approx k^{-5/3}$ and $e(k) \approx k^{-8/3}$, and one at low wavenumbers, where E cascades to larger scales, with $v \approx k^{-1}$ and $e \approx k^{-2}$. The variance of the surface flow, $\{u^2+v^2\}$, has the same spectral shape as V. The spectral slope of the cascading scalar at small scales is expected to be steeper than in two-dimensional flows ($-\frac{5}{3}$ as opposed to -1), but the variance of the flow itself should be less steep ($-\frac{5}{3}$ as opposed to -3). Numerical experiments described in PHS at 512×512 resolution confirm these qualitative predictions.

Owing to the locality of the interactions in SQG, one might expect the inertial ranges to be more easily simulated than in the two-dimensional Euler case, in which it has been notoriously difficult to obtain convergent results with increasing resolution. However, PHS find approximately the same order of discrepancy in two-dimensional and SQG models between the predicted slopes for the direct cascade and those obtained numerically. (Borue 1994 has recently found a clear k^{-1} enstrophy cascading range for two-dimensional flow in a 4096×4096 spectral model, and it will be interesting to solve the SQG equations at the same resolution.)

PHS also examine a generalization of SQG, in which the relation between the streamfunction and the advected tracer in the spectral domain is

$$\Theta_{\boldsymbol{K}} = -|\boldsymbol{K}|^{\alpha}\,\Psi_{\boldsymbol{K}}, \tag{29}$$

so that $\alpha = 1$ and 2 correspond to SQG and two-dimensional flow respectively. Their results show that the prediction of the direct inertial range spectral shape clearly breaks down as α increases beyond 2. In fact, the simulated slope for $\alpha = 3$ is similar to that for $\alpha = 2$. It appears that $\alpha = 2$ may be a special point, marking the boundary between flows for which the Kolmogorov–Kraichnan predictions for the direct cascade are satisfied, at least approximately, and flows in which the interactions are so non-local that spectra are better described by Batchelor's predictions for a passive tracer.

Figure 10(*a*) is a snapshot of the Θ-field in the SQG simulation of PHS, in which the flow is maintained by forcing at large scales (wavenumbers 4–6). The corresponding vorticity field, $(\partial_{xx}+\partial_{yy})\,\Psi$, is shown in figure 10(*b*), where only values larger than a threshold value are shaded. This vorticity field is of interest when one considers the

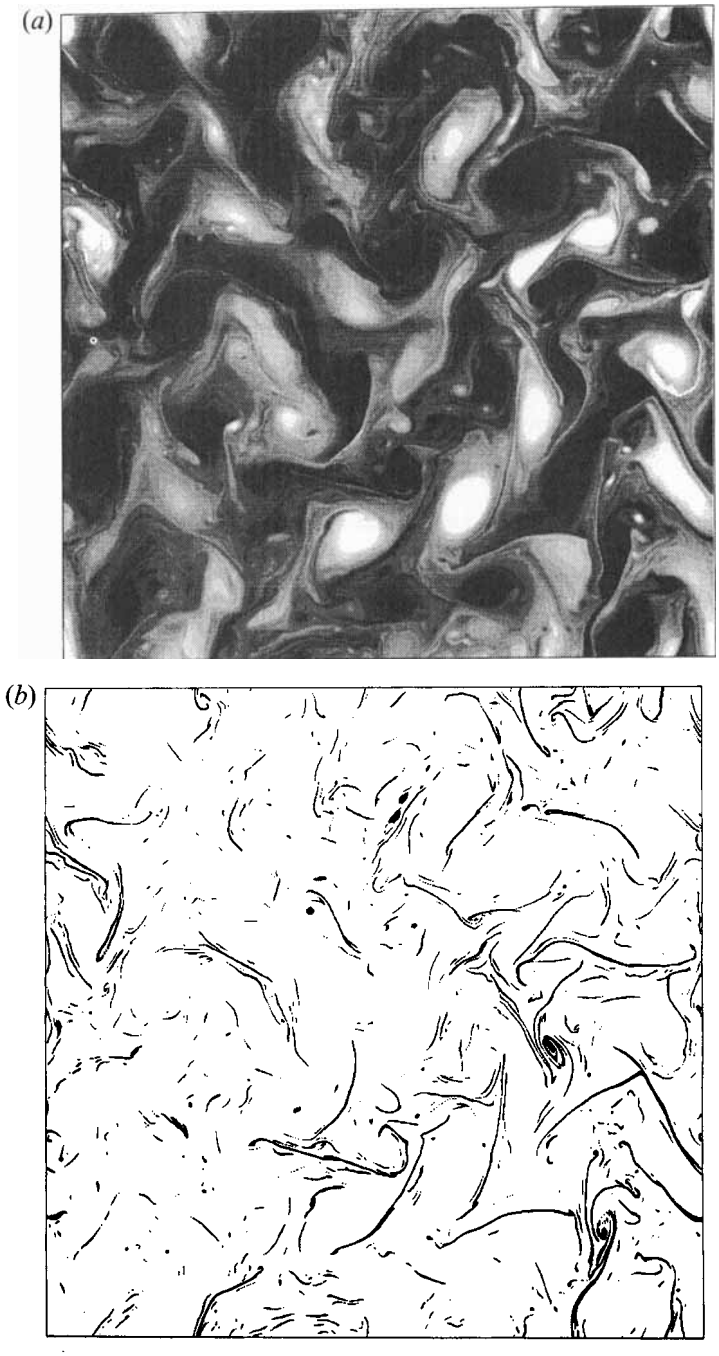

FIGURE 10. Snapshot from a forced homogeneous turbulence simulation in SQG: (*a*) temperature; (*b*) vorticity with only those points with values larger than a critical value shaded.

geostrophic momentum (GM) equations (Hoskins 1975). In this extension of quasi-geostrophic theory, one approximates the momentum by the momentum of the geostrophic flow, but advects it with the full, geostrophic plus ageostrophic, flow. It turns out that the GM equations can be solved by transforming to 'geostrophic

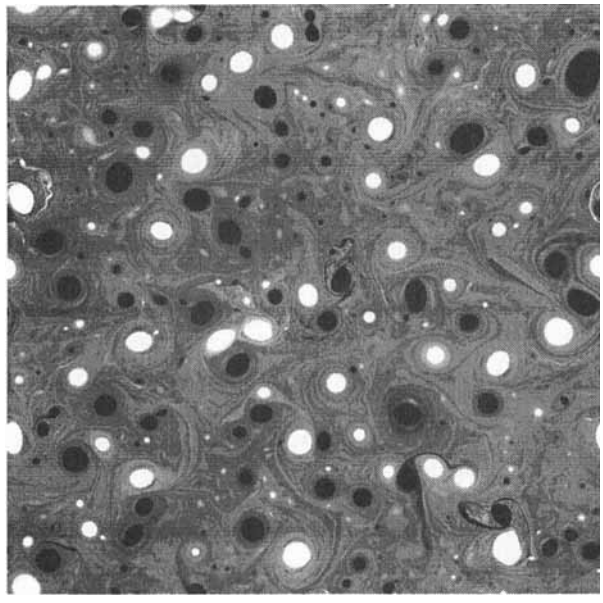

FIGURE 11. Snapshot of temperature in an unforced, decaying SQG turbulence simulation, with white noise initial condition.

coordinates' in which coordinate system the equations simply reduce to quasi-geostrophy. Therefore, one can take a quasi-geostrophic solution, such as that in figure 10, and transform it into a solution of the GM equations. The Jacobian of the transformation is essentially $1-\zeta/f$, where ζ is the vorticity displayed in figure 10(*b*). When the Rossby number ζ/f reaches unity, GM predicts the formation of a frontal singularity. The implication of figure 10 is that one can anticipate a filigree of micro-frontal singularities in homogeneous turbulent simulations of the geostrophic momentum equations. The possibility that the quasi-geostrophic equations themselves would also form such a pattern of discontinuities has been raised by Constantin *et al.* (1994). But GM predicts that the flow will develop a singularity well before the SQG equations do.

The inverse energy cascade in SQG appears to have much in common with that in the two-dimensional case. Figure 11 is a snapshot from the free evolution of an SQG flow with an initial white noise temperature field. (The scale-selective diffusivity is once again $\nabla^8 T$.) Vortices form as the cascade proceeds, more or less as in two dimensional flow (e.g. McWilliams 1984), and the evolution can be thought of as the movement of the vortices in the flow field induced by other vortices, with occasional intense encounters. There is considerable pairing of vortices and the sporadic formation of larger groups, but we have not yet attempted to determine whether there is a greater tendency for the formation of assemblages than in two-dimensions, as suggested by the discussion in §3. A qualitative difference hinted at by this figure is that vortex encounters are more violent than in two-dimensional flow: rather than merger accompanied by the formation of relatively passive filaments, encounters such as that seen on the left edge of the domain are almost invariably accompanied by the formation of small satellite vortices, through the filamentary instabilities described above. The formation of these satellite vortices should modify the evolution of the vortex size probability distribution in important ways.

Rhines (1975) has discussed the way in which the inverse energy cascade in two-

dimensional flow is halted by the presence of an environmental vorticity gradient, the beta-effect (see also Vallis & Maltrud 1992). In the two-dimensional case, within the $K^{-5/3}$ inverse energy cascade range the characteristic inverse timescale, or advective frequency, of an eddy with wavenumber $K = (k^2 + l^2)^{1/2}$ is

$$\omega_{ad} = (K^3 E(K))^{1/2} \propto K^{2/3}.$$

Comparing with the Rossby wave dispersion relation, $\omega_R = -\beta k/K^2$, one sees that wave dispersion will eventually dominate, except along the $k = 0$ axis. The transition is a fairly sharp one: $\omega_R/\omega_{ad} \approx k^{-5/3}$ for $l = 0$.

In the SQG case, the surface flow and buoyancy are predicted to have a K^{-1} spectral shape, so that $\omega_{ad} \propto K$. The edge wave frequency is $\omega_e = -Ak/K$, giving the ratio $\omega_e/\omega_{ad} \propto k^{-1}$ for $l = 0$. Thus, we still expect a transition between turbulent and wave-like behaviour, but a more gradual one, with increasing scale. Numerical experiments in which the inverse energy cascade is arrested with an environmental temperature gradient have yet to be performed.

6. Concluding remarks

An assortment of results from the SQG model have been presented which demonstrate the distinctive characteristics of its flows, and its potential importance as a numerically tractable turbulence model. As contrasted with two-dimensional flows, the shorter-range interaction leads to a turbulent cascade that more closely resembles that described in Richardson's famous ditty: 'big whorls have little whorls...'.

We have said relatively little about physical applications. One difficulty is that the cascade to smaller scales in SQG is invariably marked by increasing Rossby numbers, since it is temperature, not vorticity, that is conserved. Since vorticity involves an additional horizontal derivative, it increases as the scale is reduced. QG theory is only valid for small Rossby numbers, so these equations are self-consistent over a large spectral range only if the Rossby number of the energy-containing eddies is very small. In the atmosphere, one has at best a Rossby number of 0.1 and one decade of quasi-geostrophic scales of motion. In addition, as the horizontal scale decreases, so does the vertical scale of the SQG flow, eventually submerging the eddy in the planetary boundary layer, where the flow is strongly damped and geostrophy breaks down in any case.

Juckes (1994) has argued that SQG dynamics is relevant for tropopause perturbations (see §2). This appears to be a better candidate than the solid surface, since one no longer has to deal with the frictional effects in the planetary boundary layer, at least. However, the model can only be relevant over a fairly narrow spectral range once again, because of the size of the Rossby number in the atmosphere. Also, the approximations inherent in QG theory break down at the tropopause as soon as vertical displacements of fluid particles become substantial: for example, the familiar phenomenon of tropopause folding cannot easily be described within QG theory. Garner *et al.* (1993) describe a flow for which the breakdown of SQG is clear. The implications of SQG theory for tropopause dynamics remain to be clarified.

The range of nearly geostrophic scales in the oceans is larger than in the atmosphere. While interior potential vorticity may always be present, it need not dominate the surface temperature evolution. The interior potential vorticity should produce an enstrophy cascade similar to that in two-dimensional flow, which yields a flow spectrum that is steeper than the SQG cascade at the surface (k^{-3} as opposed to $k^{-5/3}$). Therefore, if allowed to proceed through a substantial cascade, the flow induced by the

surface temperature should dominate on small enough scales. A complex pattern of frontal structures, such as that seen in figure 10, should result. The analysis of oceanic surface temperature fields may uncover some SQG-like features.

We thank M. Juckes and A. Majda for helpful conversations on this topic. R.T.P. and K.L.S. were supported by NSF Grant ATM 89-20589.

REFERENCES

BELAND, M. 1976 Numerical study of the nonlinear Rossby wave critical level development in a barotropic flow. *J. Atmos. Sci.* **33**, 2066–2078.

BENNETT, A. F. & KLOEDEN, P. E. 1980 The simplified quasi-geostrophic equations: existence and uniqueness of strong solutions. *Mathematika* **27**, 287–311.

BENNETT, A. F. & KLOEDEN, P. E. 1982 The periodic quasi-geostrophic equations: existence and uniqueness of strong solutions. *Proc. R. Soc. Edin.* **91A**, 185–203.

BLUMEN, W. 1978 Uniform potential vorticity flow. Part I. Theory of wave interactions and two-dimensional turbulence. *J. Atmos. Sci.* **35**, 774–783.

BORUE, V. 1994 Spectral exponents of enstrophy cascade in stationary two-dimensional homogeneous turbulence. *Phys. Rev. Lett.* **72**, 1475.

CONSTANTIN, P., MAJDA, A. J. & TABAK, E. G. 1994 Singular front formation in a model for quasi-geostrophic flow. *Phys. Fluids* **6**, 9–11.

DRITSCHEL, D. G. 1988 The repeated filamentation of two-dimensional vorticity interfaces. *J. Fluid Mech.* **194**, 511–547.

DRITSCHEL, D. G. 1989*a* Contour dynamics and contour surgery: numerical algorithms for extended, high-resolution, modeling of vortex dynamics in two-dimensional, inviscid incompressible flows. *Comput. Phys. Rep.* **10**, 77–146.

DRITSCHEL, D. G. 1989*b* On the stabilization of a two-dimensional vortex strip by adverse shear. *J. Fluid Mech.* **206**, 193–221.

EADY, E. J. 1949 Long waves and cyclone waves. *Tellus* **1**, 33–52.

GARNER, S., NAKAMURA, N. & HELD, I. M. 1992 Nonlinear equilibration of two-dimensional Eady waves: a new perspective. *J. Atmos. Sci.* **49**, 1984–1996.

HOSKINS, B. J. 1975 The geostrophic momentum approximation and the semi-geostrophic equations. *J. Atmos. Sci.* **32**, 233–242.

HOYER, J.-M. & SADOURNY, R. 1982 Closure models for fully developed baroclinic instability. *J. Atmos. Sci.* **39**, 707–721.

JUCKES, M. 1994 Quasi-geostrophic dynamics of the tropopause. *J. Atmos. Sci.* **51**, 2756–2768.

KILLWORTH, P. D. & MCINTYRE, M. E. 1985 Do Rossby-wave critical layers absorb, reflect, or overreflect? *J. Fluid Mech.* **161**, 449–492.

KNOBLOCH, E. & WEISS, J. B. 1987 Chaotic advection by modulated traveling waves. *Phys. Rev.* A **36**, 1522–1524.

MCWILLIAMS, J. 1984 The emergence of isolated coherent vortices in turbulent flow. *J. Fluid Mech.* **146**, 21–43.

MILLER, J. 1990 Statistical mechanics of Euler equations in two dimensions. *Phys. Rev. Lett.* **65**, 2137–2140.

PEDLOSKY, J. 1979 *Geophysical Fluid Dynamics*. Springer.

PIERREHUMBERT, R. T. 1991 Chaotic mixing of tracers and vorticity by modulated traveling Rossby waves. *Geophys. Astrophys. Fluid Dyn.* **59**, 285–320.

PIERREHUMBERT, R. T. 1994 Tracer microstructure in the large-eddy dominated regime. *Chaos, Solitons, and Fractals* **4**, 1091–1110.

PIERREHUMBERT, R. T., HELD, I. M. & SWANSON, K. 1994 Spectra of local and nonlocal two dimensional turbulence. *Chaos, Solitons, and Fractals* **4**, 1111–1116 (referred to herein as PHS).

POZRIKIDIS, P. & HIGDON, J. J. L. 1985 Nonlinear Kelvin–Helmholtz instability of a finite vortex layer. *J. Fluid Mech.* **157**, 225–263.

RHINES, P. B. 1975 Waves and turbulence on a beta-plane. *J. Fluid Mech.* **69**, 417–443.

RHINES, P. B. & YOUNG, W. R. 1982 Homogenization of potential vorticity in planetary gyres. *J. Fluid Mech.* **122**, 347–367.

RIVEST, C., DAVIES, C. & FARRELL, B. 1992 Upper tropospheric synoptic-scale waves. 2. Maintenance and excitation of quasi-modes. *J. Atmos. Sci.* **49**, 2120–2138.

RIVEST, C. & FARRELL, B. 1992 Upper tropospheric synoptic-scale waves, 1. Maintenance as Eady normal modes. *J. Atmos. Sci.* **49**, 2108–2119.

ROSE, H. A. & SULEM, P. L. 1978 Fully developed turbulence and statistical mechanics. *J. Phys. Paris* **47**, 441–484.

SCHAR, C. & DAVIES, H. C. 1990 An instability of mature cold front. *J. Atmos. Sci.* **47**, 929–950.

SMITH, R. B. 1984 A theory of lee cyclogenesis. *J. Atmos. Sci.* **41**, 1159–1168.

THOMPSON, L. & FLIERL, G. R. 1993 Barotropic flow over finite isolated topography: steady solutions on the beta plane and the initial value problem. *J. Fluid Mech.* **250**, 553–586.

VALLIS, G. K. & MALTRUD, M. E. 1993 Generation of mean flows and jets on a beta plane and over topography. *J. Phys. Oceanogr.* **23**, 1346–1362.

WAUGH, D. & DRITSCHEL, D. G. 1991 The stability of filamentary vorticity in two-dimensional geophysical vortex-dynamics models. *J. Fluid Mech.* **231**, 575–598.

WEISS, J. B. & KNOBLOCH, E. 1988 Mass transport and mixing by modulated travelling waves. *Phys. Rev.* A **40**, 2579–2589.